EMBRY-RIDDLE Aeronautical University SCHOLARLY COMMONS

Beyond: Undergraduate Research Journal

Volume 3 Article 1

April 2019

Comparison of Terrain Effects in Divergent versus Non-Divergent Barotropic Models

Tyler E. Green
Embry-Riddle Aeronautical University, greent12@my.erau.edu

Thomas A. Guinn
Embry-Riddle Aeronautical University - Daytona Beach, guinnt@erau.edu

UNDERGRADUATE RESEARCH JOURNAL
Beyond

Comparison of Terrain Effects in Divergent versus Non-Divergent Barotropic Models

Tyler E. Green & Thomas A. Guinn

Abstract

The effects of including terrain in divergent and non-divergent, single-level barotropic models are examined in detail using a global spectral model. The non-divergent model solves the barotropic vorticity equation, while the divergent model solves the shallow water equations. In both models, the impact of terrain is evaluated by examining the evolution of the predicted heights of a pressure surface. Four simulations with initially zonal flow were run for each model using a two-dimensional Gaussian mountain shape for terrain, with two different mean fluid depths of 5,000 m and 7,500 m, and two different peak mountain heights of 2,000 m and 4,000 m. One additional simulation was completed using real North American terrain, also with initially zonal flow. As the mean fluid depth was decreased, greater differences in the predicted height fields between the two models were observed, with the shallow water model producing a more amplified leeside trough. The differences are caused by increased convergence downstream of the terrain in the shallow water model compared to the barotropic vorticity equation model as the mean fluid depth is decreased. As the mean fluid depth is increased in the shallow water model, the two different models show little difference.

Introduction

Barotropic models are one of the simplest of meteorological models and were the first used for successful numerical weather prediction in the early 1950's (Charney et al, 1950). Single-level barotropic models are broken into two categories: barotropic vorticity equation (BVE) models and shallow water models (SWMs), also known as barotropic primitive equation models (American Meteorological Society, 2018). Barotropic models assume the velocity of the atmospheric winds are constant with height. Although this assumption is limiting considering the chaotic and non-linear nature of Earth's atmosphere, they have proved valuable for studying fundamental atmospheric motions because of their simplicity. Bolin (1955) stated, "Above all it is important to start from the simplest possible idea about the dynamics of the atmosphere and gradually proceed to more complicated models. In doing so we can get a better understanding of the relative importance of various processes in the atmosphere. In that sense the barotropic model offers an excellent starting point." Because of this, barotropic models continue to be widely used to study a variety of phenomena, especially those related to tropical systems (e.g., Nieto-Ferreia and Schubert, 1997; Schubert et al, 1999; Hendricks et al, 2010; Hendricks et al, 2016).

In this paper, these two aforementioned barotropic models are used to study orographic Rossby waves, and the barotropic potential vorticity equation (1) offers a simple explanation for the formation of these waves.

$$\frac{D_h}{Dt}\left(\frac{\zeta_g + f}{h}\right) = 0 \qquad (1)$$

In a barotropic fluid, potential vorticity $\left(\frac{\zeta_g + f}{h}\right)$ is materially conserved following the fluid. In (1), ζ_g represents geostrophic relative vorticity, f is the Coriolis parameter given by $2\Omega\sin\phi$, where Ω is the Earth's angular velocity and ϕ is latitude, h represents the height of the fluid's free surface above a specified reference level, and $D_h(\,)/Dt$, is the horizontal material derivative following the fluid motion. Due to conservation of potential vorticity, as air passes over the leeside of a mountain, the height between the Earth's surface and the free surface increases causing an increase in the fluid's relative vorticity, which generates a "leeside trough" downwind of mountain ranges (Holton, 1992).This phenomenon can lead to surface leeside cyclogenesis and is partly responsible for the creation of surface lows downwind of the Rocky Mountains that play in an important role in the formation of severe weather in the U.S. Great Plains.

In the late 1950's and early 1960's, the atmospheric modeling community attempted to include terrain effects and surface friction in barotropic models because forecasts made without these effects consistently produced errors in mountainous regions (Cressman,1958; 1960). As barotropic models started

to give way to more complex models such as multi-level primitive equation models, the inclusion of topography in single-level barotropic models seemingly went by the wayside, as newer multi-level models include topography in a more natural manner.

A review of the literature suggests there has been no study comparing the effects of terrain in a single-level non-divergent barotropic model (i.e., BVE model) versus a single-level divergent model (i.e., SWM). In fact, there are no studies in the meteorological literature that include terrain effects in SWMs. This is likely due to two reasons, the difficulty of initializing a SWM with terrain while suppressing unwanted gravity waves, and the modeling community's desire to develop, as quickly as possible, more complex primitive equation models capable of representing multiple vertical levels. Therefore, the purpose of this paper is to investigate the inclusion of topography in these two single-level barotropic models to find any differences in the flow evolution, since the inclusion of terrain is fundamentally different for each.

The remainder of the paper is structured in the following way. The Model Development and Methods Section provides the methods used in the study and provides a detailed description of the equations for the two different models as well as a detailed discussion of the differences in how terrain topography is incorporated in the model equations. In the Results Section, we present the output from four different idealized simulations using two different fluid depths (for the SWM), two different idealized topographical mountains, and one simulation using actual North American topography. In the Discussion Section, we offer insight as to why differences between the model simulations occur.

Model Development and Methods

The incorporation of terrain is uniquely different between the BVE and SWM. So before describing the experiments, we first provide a detailed discussion of the model basics as well as how the effects of terrain are incorporated into each respective model.

Quasi-Geostrophic BVE (Non-Divergent Barotropic Case)

To obtain the form of the BVE used in this study, we start with the barotropic potential vorticity equation (Holton, 1992).

$$\frac{D_h(\zeta+f)}{Dt}=\frac{\partial\zeta}{\partial t}+\boldsymbol{V}_h\bullet\nabla(\zeta+f)=-(\zeta+f)\nabla\bullet\boldsymbol{V}_h \quad (2)$$

In (2), V_h represents the horizontal wind vector, ζ is the vertical component of relative vorticity, and f is the Coriolis parameter. Using the mass continuity equation in isobaric coordinates:

$$\frac{\partial\omega}{\partial p}=-\nabla\bullet\boldsymbol{V}_h \quad (3)$$

where $\omega=Dp/Dt$ is vertical velocity and p is pressure, (2) can be rewritten as:

$$\frac{D(\zeta+f)}{Dt}=\frac{\partial\zeta}{\partial t}+\boldsymbol{V}_h\bullet\nabla(\zeta+f)=(\zeta+f)\frac{\partial\omega}{\partial p} \quad (4)$$

Equation (4) states that following the motion of an air parcel, the only mechanism that can change the parcel's total vorticity ($\zeta+f$) is horizontal velocity divergence or convergence. The right-hand side (RHS) of this equation is usually referred to as the "divergence term" or "stretching term," and for the purposes of this study, this term must be expressed in terms of terrain. Before this is done, we simplify the RHS of (4) by replacing the absolute vorticity ($\zeta+f$) by the Coriolis parameter solely. On the synoptic scale, this assumption can be made by performing a scale analysis, which shows relative vorticity is usually much less than Coriolis parameter in magnitude. This same assumption is commonly made when deriving the quasi-geostrophic vorticity equation (e.g., Lackmann, 2012; Holton, 1992). The barotropic assumption is then made by integrating both sides of equation (4) in pressure assuming the wind is invariant with height, and that the vertical velocity vanishes when pressure equals zero (i.e., ω(0)=0):

$$\int_0^{p_s}\frac{\partial\zeta}{\partial t}+\boldsymbol{V}_h\bullet\nabla(\zeta+f)\,dp=\int_0^{p_s}f\frac{\partial\omega}{\partial p}dp, \quad (5)$$

where p_s represents the surface pressure. From this equation we obtain the barotropic vorticity equation:

$$\frac{\partial\zeta}{\partial t}+\boldsymbol{V}_h\bullet\nabla(\zeta+f)=f\frac{\omega_s}{p_s} \quad (6)$$

To obtain an equation that includes terrain, we need to represent the RHS of (6) with the spatial gradient of terrain. To do so, we expand the surface vertical velocity, ω_s, in height coordinates below:

$$\omega_s=\frac{Dp_s}{Dt}=\frac{\partial p_s}{\partial t}+\boldsymbol{V}\bullet\nabla p_s \quad (7)$$

In a BVE model, the total mass of the fluid above a point at the Earth's surface never changes with time. Because of this, the local time rate of change of surface pressure is set to zero in (7), which is the same technique used in DeCaria and Van Knowe (2014). Equation (7) is then reduced to the following:

$$\omega_s = \frac{Dp_s}{Dt} = \boldsymbol{V} \bullet \nabla p_s \tag{8}$$

Lastly using the hydrostatic relationship:

$$\nabla p = -\rho g \nabla z \,, \tag{9}$$

where ρ represents air density and z is the height of the pressure surface, combined with the equation of state, the final version of the BVE used in this study is given below.

$$\frac{\partial \zeta}{\partial t} + \boldsymbol{V} \bullet \nabla \left(\zeta + f \right) = -\frac{gf}{R_d T_s} \boldsymbol{V} \bullet \nabla z_s \tag{10}$$

In (10), g is gravity, R_d is the gas constant for dry air, T_s is the surface temperature of Earth, and z_s is the surface (terrain) height. The last forcing term on the RHS of (10) is a parameterization of the "divergence" term from the vorticity equation, and it represents how flow over sloped terrain can modify relative vorticity with time. A similar form of (10) was used for the first successful instance of numerical weather prediction (Charney, 1950). The BVE is referred to as a "filtered equation," meaning it does not support gravity or acoustic waves as solutions, leaving Rossby waves as solutions (Decaria and Van Knowe, 2014). Gravity waves, for example, are not usually of meteorological interest on synoptic scales, and are therefore not of interest for this study. However, they are supported in the SWM equations, which are discussed next.

SWM (Divergent Barotropic Case)

The SWM equations consist of a set of three prognostic equations, one each for divergence, vorticity, and geopotential height. These three equations stem from the Navier-Stokes and mass continuity equations for a homogeneous, incompressible, inviscid, and hydrostatic fluid (Hack and Jakob, 1992). These two equations, respectively, are presented below.

$$\frac{D_h \boldsymbol{V}}{Dt} = -f\hat{\boldsymbol{k}} \times \boldsymbol{V} - \nabla \Phi \tag{11}$$

$$\frac{\partial w}{\partial z} = -\nabla \bullet \boldsymbol{V} \tag{12}$$

In equations (11) and (12), Φ represents the geopotential of the pressure surface above some reference height, and $w=Dz/Dt$ is the vertical velocity of the free surface. To obtain the vorticity equation, the vertical component of the curl of equation (11) is taken:

$$\frac{\partial \zeta}{\partial t} = -\nabla \bullet \left(\zeta + f \right) \boldsymbol{V} \tag{13}$$

To obtain the divergence equation, the horizontal divergence of equation (11) is taken:

$$\frac{\partial \delta}{\partial t} = \hat{\boldsymbol{k}} \bullet \nabla \times \left(\zeta + f \right) V - \nabla^2 \left(\Phi + \frac{\boldsymbol{V} \bullet \boldsymbol{V}}{2} \right) \tag{14}$$

In the above equation δ represents horizontal divergence. To obtain the tendency equation for Φ, the continuity equation (12) is integrated from the terrain height (z_s) above some reference level (taken to me MSL in this study) to the height of the free surface (η), while again assuming a barotropic atmosphere.

$$\int_{z=z_s}^{z=\eta} \frac{\partial w}{\partial z} dz = \int_{z=z_s}^{z=\eta} -\nabla \bullet \boldsymbol{V} dz \tag{15}$$

Performing this integration and simplifying, the continuity equation gives a time tendency equation for the perturbation geopotential of the free surface that includes terrain. (See Appendix A for complete derivation).

$$\frac{\partial \Phi'}{\partial t} = -\nabla \bullet \left[(\Phi' - g z_s) \boldsymbol{V} \right] - \bar{\Phi} \delta \tag{16}$$

In (16), Φ' is the perturbation geopotential of the pressure surface from the mean state, $\bar{\Phi}$, which is also representative of the mean depth of the pressure surface. Equations (13), (14), and (16) make up the prognostic equations for the SWM used in this study.

The SWM equations are also referred to as the barotropic primitive equations because they contain prognostic equations for vorticity, divergence, and the height of a free pressure surface. In addition, these equations are often referred to as "unfiltered" because they support gravity-wave solutions. Special care must be taken in the initialization of the SWM to ensure gravity waves are not prominent in the model's solution, leaving Rossby waves as the dominant feature.

Once again, our goal is to evaluate differences in the forecasts of a single pressure surface using the BVE vs the SWM when terrain is present. Although both sets of equations are barotropic, they differ significantly in how

they represent divergence. The BVE is a single prognostic equation describing how relative vorticity changes on a free pressure surface, while the SWM describes how vorticity, divergence, and fluid depth evolve. To see how the vorticity equations for the two different frameworks differ, (13) is rewritten as:

$$\frac{\partial \zeta}{\partial t} + \boldsymbol{V} \bullet \nabla(\zeta + f) = -(\zeta + f)\nabla \bullet \boldsymbol{V} \qquad (17)$$

which is the same form of vorticity equation as (2) before vertical integration. Therefore, the difference between the BVE (10) and the vorticity equation of the SWM (17) lies in the "divergence term." For the BVE, this term is parameterized in terms of a terrain gradient whereas in the SWM, divergence is a prognostic variable that can impact both the vorticity and geopotential tendencies. In the SWM system, the effects of terrain are incorporated in the mass continuity equation (15), which becomes the prognostic equation for the geopotential of the free surface (16).

It is also important to discuss how the results from the two models are compared, given that the BVE model predicts only relative vorticity, while the SWM predicts relative vorticity, divergence, and geopotential. *The results of the simulations will be compared using geopotential height*. To produce a geopotential height field from the results of the BVE model, the non-linear balance equation (NLBE) is solved (Hack and Jacob, 1992). This equation is discussed in more detail in the next sub-section and is provided in full in Appendix B. This method of generating a geopotential height field from the predicted variable of the barotropic vorticity equation clearly is an extra step that can generate errors in the model forecasts; however, with the simplicity of the initial fields used to test the two models (discussed in the next subsection), this method is sufficiently accurate for this study and was even used with early operational models to initialize their simulations (Charney, 1955).

Experimental Setup and Model Specifics

For this study, we performed five different simulations for both the BVE model and SWM. All of the simulations were developed using MATLAB. The BVE codes followed Krishnamurti et al (2006), while the SWM codes followed Hack and Jacob (1992). The first four simulations presented used a two-dimensional Gaussian shape as topography, while the last simulation used real terrain for North America.

The first four simulations presented in this study initialize globally zonal flow while changing both the mean depth of the fluid as well as the height of the smooth two-dimensional Gaussian shape (hereafter referred to as "Gaussian mountain") representing terrain. These four simulations were run with peak Gaussian mountain heights of 2,000 and 4,000 m, and mean fluid depths of 5,000 and 7,500 m. For each simulation, the Gaussian mountain is centered on 252˚ longitude and 40˚ latitude, placing it in the general region of the Rocky Mountains, simply for visualization purposes. The Gaussian mountain has a full-width at half maximum of 3˚ and 5˚ in the longitudinal and latitudinal directions, respectively. The mean depth of the fluid and the peak height of the Gaussian mountain were adjusted to highlight differences between the model equations. The mean depth of the fluid only plays a role in the SWM, and directly impacts the geopotential tendency, which in turn affects the divergence and vorticity tendencies. In addition, the mean depth also affects the pure gravity-wave speed. A table that summarizes the variables for the four different simulations is provided below. The simulation number corresponds to frames in Figures 1-4, looking at them from left to right, and top to bottom.

Simulation	Mean Fluid Depth	Peak Mountain Height
1	5,000 m	2,000 m
2	7,500 m	2,000 m
3	5,000 m	4,000 m
4	7,500 m	4,000 m

Table 1: Summary of mean fluid depth and peak mountain height for the four idealized simulations. Note that each of these four simulations are done for both the BVE and SWM.

By changing the peak height of the Gaussian mountain, while keeping the full width at half maximum constant, the terrain surface gradients can effectively be changed, which impacts the forcing term on the RHS of equation (10) in the BVE, as well as the first forcing term in equation (16) for the tendency of geopotential in the SWM. Because the flow is initialized as zonal, we can make comparisons in the four different simulations to analyze how changing these variables affects the structure of the orographic Rossby wave generated on the leeside of the Gaussian mountain.

For the final simulation, we initialized the model with the same zonal flow as the previous simulations but used real terrain obtained from the National Center for Environmental Information on a high

spatial-resolution grid (0.0167˚×0.0167˚). The terrain data was then bi-linearly interpolated to the model grid for use. This simulation used a mean depth of 5,640 m to approximate the height of a 500 hPa forecast. The simulations highlight differences in the two model forecasts by using terrain that is less smooth than the simple Gaussian mountain.

For both models, we used the Galerkin (spectral) method to integrate the prognostic equations on the sphere. Spherical harmonic basis functions were used to represent scalar fields on the globe. For the BVE model, the prognostic equation is transformed into a similar form as Krishnamurti et al (2006) but with an extra vorticity forcing term representing terrain. The SWM follows the development by Hack and Jakob (1992) with a modification to the prognostic equation for geopotential representing terrain effects. Each model simulation used a 256 × 156 (longitude points × latitude points) Gaussian grid with a triangular truncation of 85 (T85) to avoid aliasing errors of quadratically non-linear terms. This specified grid gives a maximum grid spacing of 1.4˚ at the equator with a maximum effective grid spacing of approximately 2˚.

For the BVE model, the initial time step is performed using a forward Euler scheme in spectral space, followed by centered-in-time integration in spectral space for all remaining time steps. A 100 s time step was used for all time steps in the BVE model. For the SWM, we used a semi-implicit scheme following Hack and Jakob (1992), where the prognostic equations for geopotential and divergence were integrated using an implicit, trapezoidal scheme, while the prognostic equation for vorticity was integrated explicitly using a centered-in-time scheme. The semi-implicit method was chosen for the SWM to avoid violating Courant-Friedrichs-Lewy (CFL) criteria for the faster, pure gravity waves. This allowed a time step approximately six times larger than the theoretical value satisfying the CFL criteria (Bourke, 1972). The initial time step for the SWM consisted of six explicit time steps of length dt/6 seconds, where dt is the time step used for the semi-implicit scheme to avoid violating the CFL criteria during these explicit steps. The remaining SWM time steps were completed using the semi-implicit method discussed above, all with 100 s time steps.

For the BVE model (10) the surface temperature in the terrain forcing term was assigned a constant value of $287K$ for all simulations used in this study. For given values of the wind magnitude and terrain gradients, the range of normal Earth temperatures would not significantly alter the magnitude of the forcing term, therefore justifying the use of a constant temperature during the simulations.

To initialize the stream function to produce globally zonal flow, we used a single term spherical harmonic expansion of rank 0 and degree 1 with an amplitude of -2×10^{10} m^2 s. This resulted in a maximum zonal wind speed of approximately 30 m s^{-1} at the equator and approximately 23 m s^{-1} at 40˚ N over the location of the Gaussian mountain peak.

In equation (18) Y represents the fully normalized

$$\psi(\lambda,\phi) = -2\times10^{10} Y_1^0(\lambda, \sin\phi) \tag{18}$$

spherical harmonic (Y_n^m), where m is the rank, n is the degree, λ represents longitude, and ϕ represents latitude.

From this streamfunction, an initial vorticity and non-divergent wind field are both easily calculated, which is done for both the BVE model and the SWM. However, for the initialization of the SWM, divergence and geopotential must also be specified before model integration. To match the initial condition in the barotropic vorticity model, the initial divergence field is set to zero. As mentioned earlier, because the SWM equations are "unfiltered" and allow gravity wave solutions, the SWM must be initialized with balance between the mass and wind fields to minimize the generation of gravity waves early in the model simulation. To initialize the geopotential field for the SWM, the NLBE is solved using the initial winds obtained from the specified streamfunction. Using the NLBE also ensures the SWM initially minimizes the *tendency* for gravity wave as well.

As mentioned earlier, one of the likely reasons there has not been research with terrain incorporated in single-level SWMs is the difficulty in initializing the model with terrain while avoiding the generation of spurious gravity waves due to the initial imbalance of the mass and wind fields. To avoid this problem, the model terrain is artificially grown over a 12-hour period using a linear combination of Hermite polynomials given below (in units of hours).

This amplitude growth function produces a smooth

$$A(t) = 1 - 3\left(\frac{12-t}{12}\right)^2 + 2\left(\frac{12-t}{12}\right)^3 \quad 0 \le t \le 12 \tag{19}$$

polynomial whose amplitude begins as 0 and takes on a value of 1 at 12 hours. Another useful property of (19) is the function's derivatives at the endpoints are both

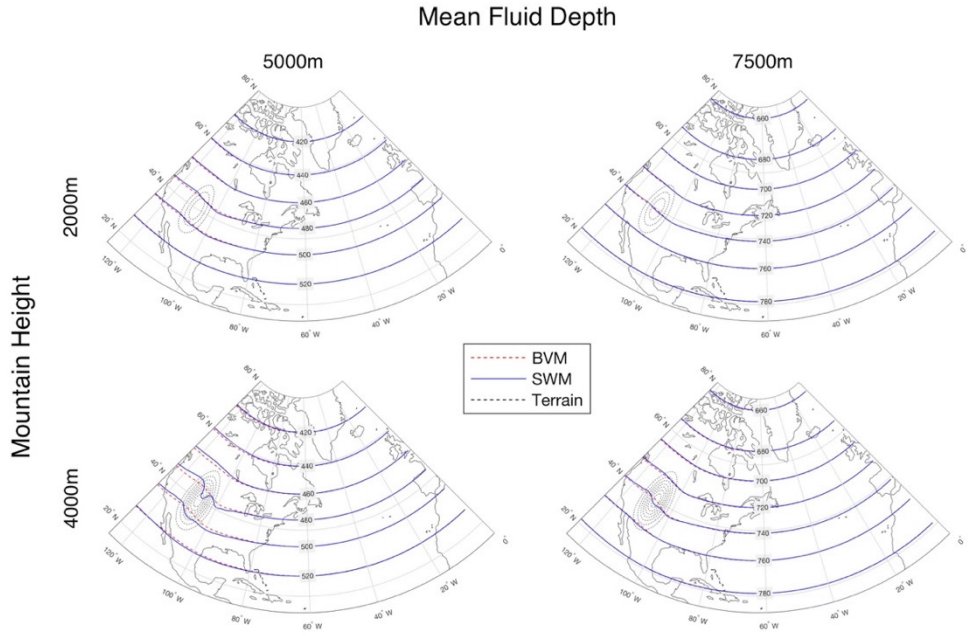

Figure 1: 12-hour forecast results from the four different simulations done with the Gaussian Mountain. All contours are in decameters.

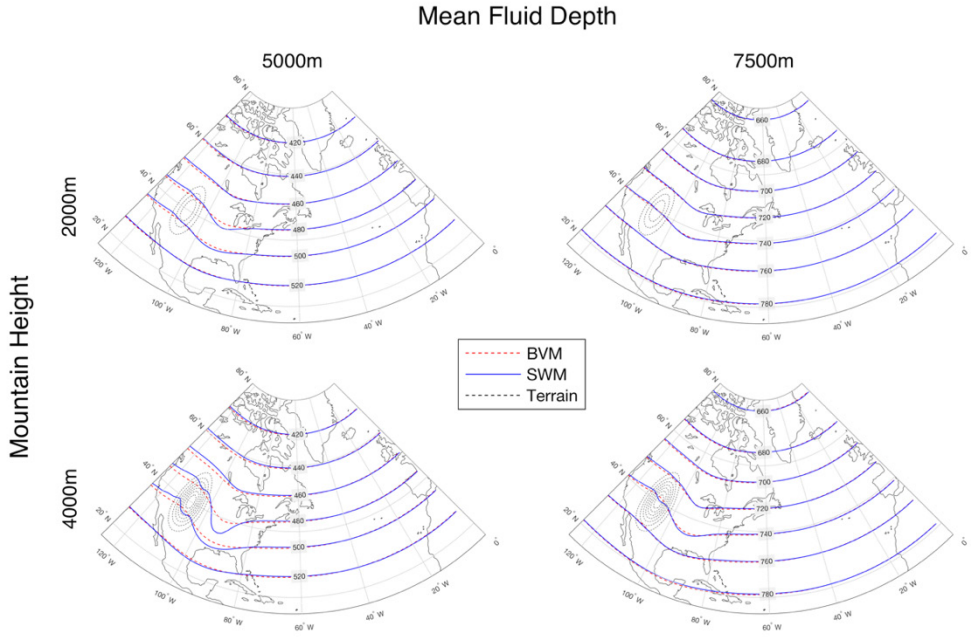

Figure 2: Same as figure 1 but for 24-hour forecast.

zero, making the mountain grow smoothly at a slow rate to start and then taper off smoothly at the end of the 12-hour period. This helps minimize the excitation of gravity waves while the terrain is being included. The results of the five simulations are presented next.

Results

Figures 1-4 compare the results of the 48-hour BVE model and SWM simulations at 12, 24, 36, and 48 hours using the following structure: the mean depth of the simulation varies horizontally across the figure, while the Gaussian mountain height varies vertically in the figure. Throughout the course of the 48-hour simulation,

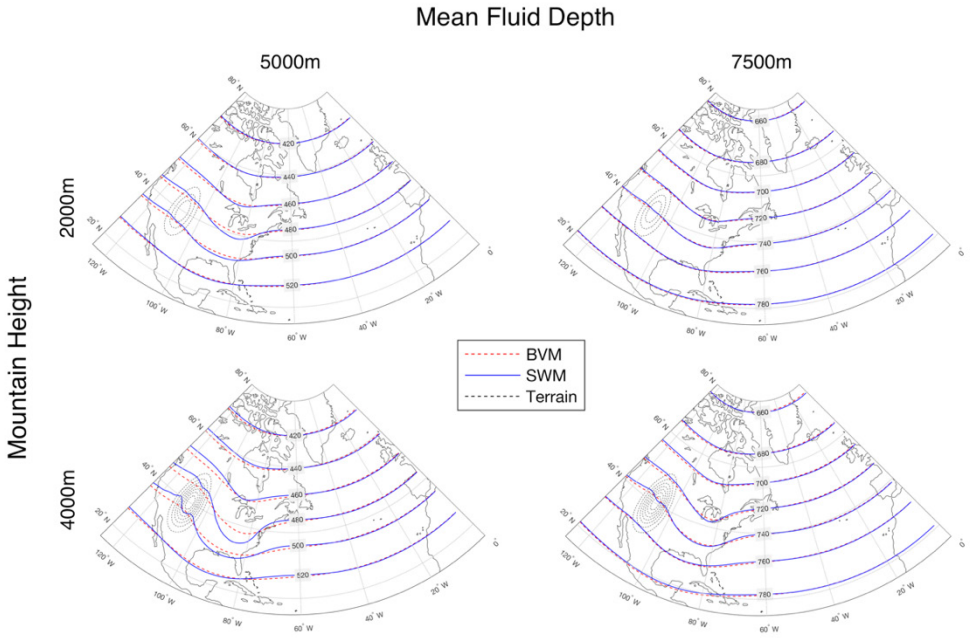

Figure 3: Same as figure 1 but for 36-hour forecast.

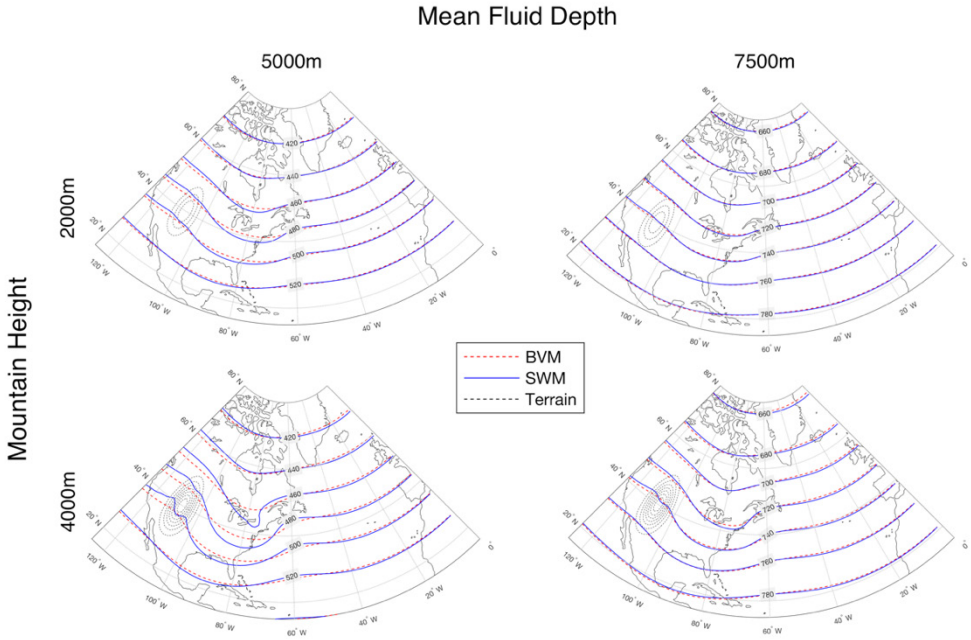

Figure 4: Same as figure 1 but for 48-hour forecast.

the most noticeable differences between the two model simulations occur for the mountain height of 4,000 m and mean fluid depth of 5,000 m, because the SWM creates a much larger amplitude leeside trough than the BVE model. Another less noticeable difference between the two model runs occurs in the simulation using a Gaussian mountain height of 2,000 m and a mean depth of 5,000 m, where the leeside trough is slightly more pronounced in the SWM than in the BVE model. Interestingly, both simulations with a mean fluid depth of 7,500 m had nearly identical results in the predicted height fields.

Examining the simulation using real terrain data for North America (Fig. 5), we see similar patterns in the predicted height field as observed in the simulation using a Gaussian mountain peak of 4,000 m and a mean depth of 5,000 m. This would be expected given the mean depth used in this simulation is 5,640 m

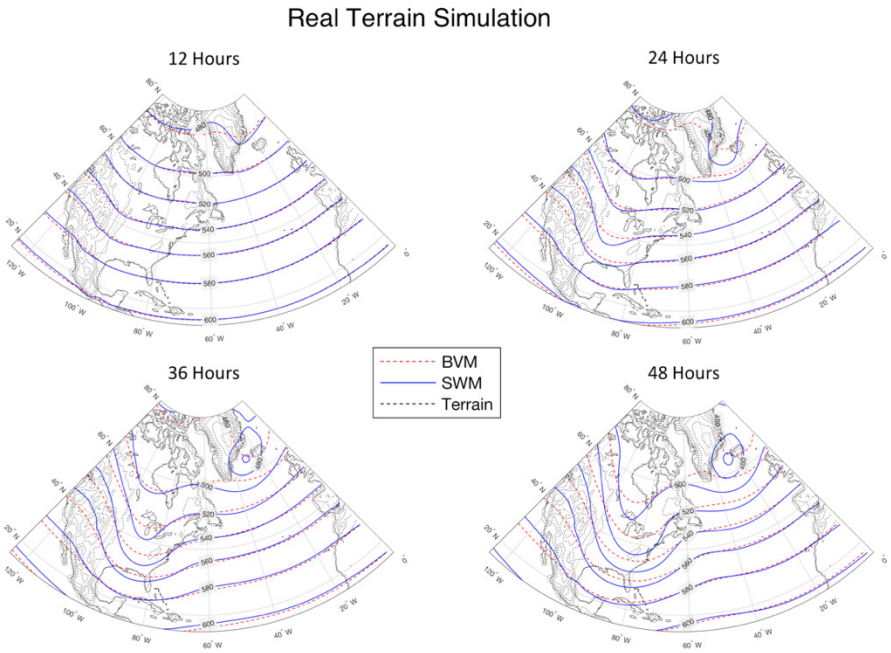

Figure 5: Results of full 48-hour simulations using real terrain for North America. All contours are in decameters.

and the maximum topography height in the Rookies is approximately 3,000 m. Just as in the previous Gaussian mountain simulation, the SWM created a more pronounced trough in the height field, even to the extent of producing a closed low-pressure center downwind of the topography in Greenland. It is also apparent that the leeside waves formed in this simulation by both models have much higher amplitudes than in any of the simulations that used a Gaussian mountain. This is likely due to the topography of the Rocky Mountains extending farther north than did the Gaussian mountain, as well as the Sierra Madre mountains extending farther south than the Gaussian mountain. Because of the spatial extent of these two mountain ranges at approximately the same longitude, a constant source of terrain-driven relative vorticity is generated to the east along the entire latitudinal extent of these ranges. The source of relative vorticity along the two mountain ranges would cause the leeside wave to continually deepen in amplitude throughout the simulation before propagating eastward.

Discussion

From the results presented in the previous section, it is apparent there is not a noticeable sensitivity of the BVE model to changing the height of the topography, as it produces similar results for both Gaussian mountain heights. There is a noticeable sensitivity in the SWM, however, to a change in the mean fluid depth (it is important to note that changing the mean fluid depth has no impact on the BVE model). When the SWM was run with a smaller mean depth (5,000 m in the idealized simulations and 5,640 m in the simulation using real terrain) and interacted with taller topography, it produced much deeper leeside waves than when a larger mean fluid depth was used. Because of this, we discuss possible reasons why changing the mean depth in the SWM causes the solutions in the two frameworks to diverge.

For simplicity, we will consider only the SWM and BVE simulations run with a Gaussian mountain peak height of 4,000 m. Examining the bottom left panel of Fig. 4, we observe that at the end of the SWM simulation with a mean depth of 5,000 m, there is a large difference between the amplitudes of the leeside troughs of the SWM and the BVE model simulations. This difference in amplitude would indicate a difference in the relative vorticity in the base of these troughs. The difference in the vorticity equations was discussed in the Methods Section, and to test how divergence is handled between the two separate frameworks' vorticity equations, the relative vorticity tendency due to the divergence term for each framework was plotted versus time for a single grid point. This point was located at 40° North and 100° West, which lies just east of the mountain. Examining Fig. 6, the relative vorticity

forcing due to divergence is stronger in the SWM simulations for both fluid depths (the BVE model has the same forcing for both simulations because it does not depend on mean depth). More specifically, looking at the left panel in Fig. 6, when the mountain reaches its peak height at 12 hours (and when the forcing for relative vorticity due to divergence reaches a maximum) the magnitude of the forcing in the SWM is approximately eight times larger than that of the BVE model. Again, it is important to note that in the BVE model, the relative vorticity term is omitted from the divergence term in the vorticity equation for synoptic scale motion (see Methods). The same test was done with the inclusion of relative vorticity in the forcing term for the BVE model, and the differences proved to be negligible (not shown). The right panel in Fig. 6 shows that even with a larger fluid depth, the forcing for relative vorticity by the divergence term is again larger in the SWM, but by a smaller margin. In addition, increasing the mean fluid depth decreases the difference between the magnitude of the forcing from the divergence term in the two frameworks. This makes the structure of the forecasted height match that of the BVE model more closely, which is evident in the two right panels of Fig. 4.

This analysis helps to explain the difference between the BVE model and SWM forecasts due to changing the mean depth. However, a more in-depth look at the sensitivity of just the SWM alone to mean fluid depth was also desired. To do this, we plotted the atmospheric divergence, along with the individual forcing terms that comprise the geopotential tendency, at two model grid points, one at 40° N and 100° W, and one at 40° N and 90° W. For each point, we used the same mean fluid depths as in the previous experiment and a Gaussian mountain height of 4,000 m. In the geopotential tendency equation (16), we refer to the first forcing term on the RHS as the mass flux term, and we refer to the second term on the RHS as the divergence term. Looking at the left two panels in Fig. 7, there is a strong negative correlation between the atmospheric divergence and geopotential tendency (divergence is negative and geopotential tendency is positive) in the 5,000 m mean depth simulation, with the divergence term accounting for most of the forcing for geopotential tendency at 40° N and 100° W. This negative correlation is also seen in the right two panels in Fig. 7, and we clearly see the magnitude of the atmospheric divergence for the simulation with mean depth of 7,500 m smaller than it was for the mean depth of 5,000 m, which therefore had a lesser impact on the geopotential forcing. We also observed the geopotential tendency at this point just downwind of the mountain was positive, which is consistent with the bottom left panels of Figs. 1-4, where height rises were found.

Examining Fig.8, which plots the same variables as discussed above but at 40° N and 90° W (which is aligned better with the track of the leeside trough) this negative correlation between the atmospheric divergence and the geopotential tendency is seen again (divergence is positive and geopotential tendency is negative). In both bottom panels, atmospheric divergence is

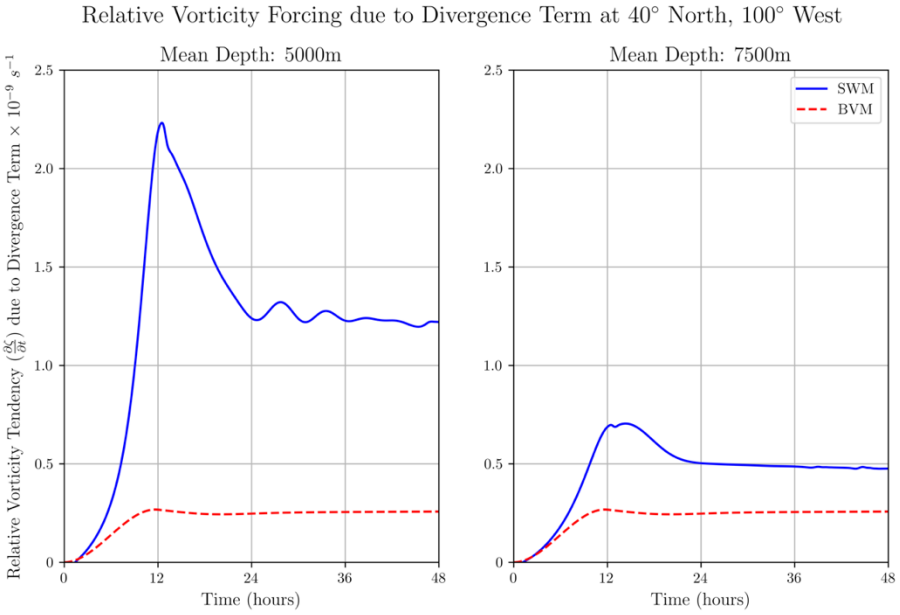

Figure 6: Comparison of vorticity tendency due to the divergence term in SWM vs BVM for two different mean fluid depths and mountain peak of 4,000 m.

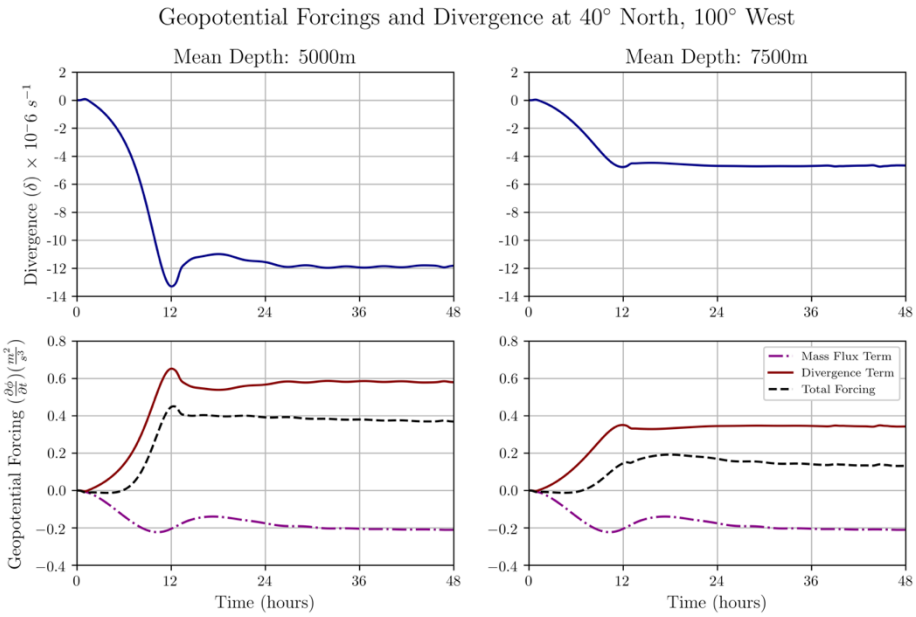

Figure 7: Comparison of atmospheric divergence and geopotential forcings for two different mean depths in the SWM. Mountain height used was 4,000 m.

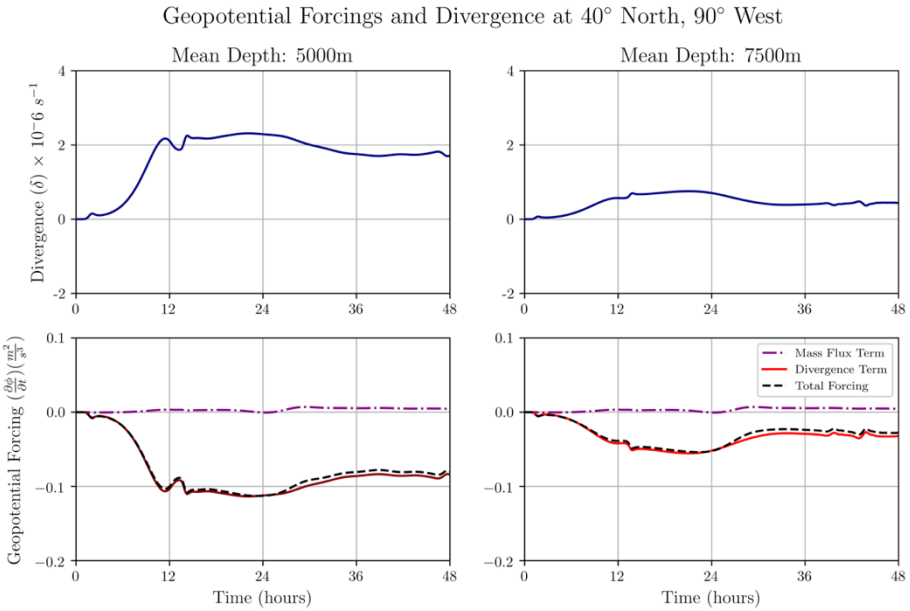

Figure 8: Comparison of atmospheric divergence and geopotential forcings for two different mean depths in the SWM. Mountain height used was 4,000 m.

controlling the geopotential tendency at this location, as the two forcing terms are similar due to the near-zero contribution of geopotential forcing from the mass flux term. The larger magnitude of divergence is seen again in the simulation with 5,000 m mean depth, which causes a larger negative geopotential tendency. This is again consistent with the height falls observed as the leeside wave moves from west to east over this point during the 48-hour simulation.

This study demonstrated clear differences in the effects of terrain in divergent and non-divergent barotropic models because the SWM can create divergence throughout the course of its simulation, while the BVE model cannot. Changing the gradient of the terrain did not have as large of effect on the differences in the simulations between the two models as did changing the mean fluid depth. This becomes especially clear as the mean depth of the SWM is decreased. The decreased fluid depth resulted in greater magnitudes of divergence generated on the leeside of terrain, which had a large impact on the height tendency. This, in turn, created deeper leeside waves. As the mean depth is increased, the results of the two models start to resemble each other very closely, which is seen in the two right panels in Figs. 1-4.

While this research has limited use in operational

forecasting, it does demonstrate the impact terrain can have on simulations attempting to isolate basic dynamical features using barotropic models. This is especially true since some SWM studies over flat terrain have used fluid depths as low as 222 m (Nieto-Ferreira and Schubert, 1997). If terrain is included, increases in the fluid depths to avoid "bottoming out" (i.e., a negative fluid depth) could lead to significantly different results, which should be considered. As mentioned in the Methods Section, using single level barotropic models offer the benefit of their simplicity. Although the model equations seem complex, the results of the simulations can be more easily explained by the model equations compared to, for example, if the full set of seven governing equations were used. However, there are more complex interactions in the atmosphere that can only be represented in a model by using multiple vertical levels. For example, in a baroclinic atmosphere (where pressure surfaces and density surfaces intersect), temperature advections occur on the pressure surface and can only be calculated if the model has two or more vertical levels. More complex non-barotropic interactions could cause the development of the orographic Rossby waves in our simulations to be much different, and in this way, our study of orographic Rossby waves is limited to only *pure* barotropic effects, which are not often observed in the real atmosphere. As Bolin stated in the quote provided in Section 1, the barotropic model is a good starting point for understanding the dynamics of the atmosphere, and that we should gradually proceed to more complicated models. The next level of complication to be added on to this work would be to use multiple vertical model levels and include baroclinic effects to analyze the impacts on how these processes change the development of these waves.

References

American Meteorological Society, 2012: Glossary of Meteorology. Accessed 22 August 2018, http://glossary.ametsoc.org/wiki/Barotropic_model

Bourke, W., 1972: An efficient, one-level, primitive-equation spectral model. *Mon. Wea. Rev.*, **100**, 683–689, https://doi.org/10.1175/1520-0493(1972)100<0683:AEOPSM>2.3.CO;2

Bolin, B. (1955), Numerical forecasting with the barotropic model. *Tellus*, **7**, 27-49, https://doi.org/10.1111/j.2153-3490.1955.tb01139.x

Charney, J. G., R. Fjortoft, and J. von Neumann, 1950: Numerical integration of the barotropic vorticity equation. *Tellus*, **2**, 237-254, https://doi.org/10.1111/j.2153-3490.1950.tb00336.x

Charney, J. G., 1955: The use of the primitive equations of motion in numerical prediction. *Tellus*, **7**, 22-26, doi:10.1111/j.2153-3490.1955.tb01138.x

Cressman, G. P., 1958: Barotropic divergence and very long atmospheric waves. *Mon. Wea. Rev.*, **86**, 293-297, https://doi.org/10.1175/1520-0493(1958)086<0293:BDAVLA>2.0.CO;2

Cressman, G. P., 1960: Improved terrain effects in barotropic forecasts. **88**, 327-342, https://doi.org/10.1175/1520-0493(1960)088<0327:ITEIBF>2.0.CO;2

DeCaria, A. J., and G. E. Van Knowe, 2014: *A First Course at Atmospheric Modeling*, Sundog Publishing, 320 pp.

Holton, J. R., 1992: *An Introduction to Dynamic Meteorology*, 3rd ed., Academic Press, 511 pp.

Krishnamurti, T. N., H. S., Bedi, V. Hardiker, and L. Watson-Ramaswamy, 2006: *An Introduction to Global Spectral Modeling*. Springer-Verlag, NY, 320 pp.

Lackmann, G., 2012: *Midlatitude Synoptic Meteorology*. American Meteorological Society, 345 pp.

Hack, J. J., and R. Jakob, 1992: *Description of a Global Shallow Water Model Based on the Spectral Transform Method*. NCAR Technical Note NCAR/TN-343+STR, http://dx.doi.org/10.5065/D64B2Z73

Hendricks, E. A., W. H. Schubert, S. R. Fulton, and B. D. McNoldy, 2010: Spontaneous-adjustment emission of inertia-gravity waves by unsteady vortical motion in the hurricane core. *Quart. J. Roy. Meteorol. Soc.*, **136**, 537-548, doi:10.1002/qj.547

Hendricks, E. A., M. A. Kopera, F. X. Giraldo, M. S. Peng, J. D. Doyle, and Q. Jiang, 2016: Evaluation of the utility of static and adaptive mesh refinement for idealized tropical cyclone problems in a spectral element shallow-water model. *Mon. Wea. Rev.*, **144**, 3697-3724, https://doi.org/10.1175/MWR-D-15-0146.1

Nieto Ferreira, R., and W. H. Schubert, 1997: Barotropic aspects of ITCZ breakdown. *J. Atmos. Sci.*, **54**, 261-285, doi.org/10.1175/1520-0469(1997)054<0261:BAOIB>2.0.CO;2

Schubert, W. H., M. T. Montgomery, R. K. Taft, T. A. Guinn, S. R. Fulton, J. P. Kossin, and J. P. Edwards, 1999: Polygonal eyewalls, asymmetric eye contraction, and potential vorticity mixing in hurricanes. *J. Atmos. Sci.*, **56**, 1197-1223, doi.org/10.1175/1520-0469(1999)056<1197:PEAECA>2.0.CO;2

Appendix A

Derivation of the Geopotential Tendency Equation with Inclusion of Bottom Topography

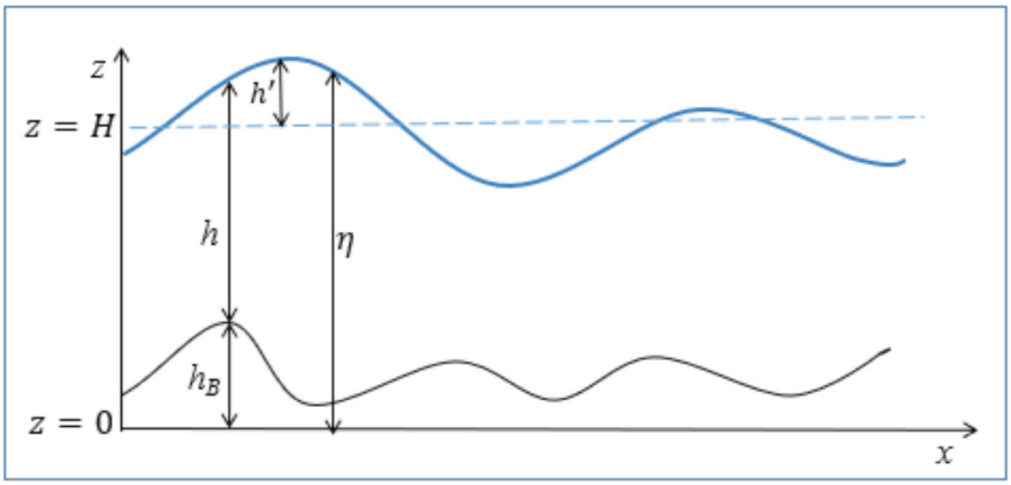

Figure A.1: Shallow water cross section showing different variables for the inclusion of terrain.

To derive the geopotential tendency equation with bottom topography, we first start with a statement of the incompressible continuity equation, where w is the vertical velocity of the free surface, ∇ is the horizontal gradient operator, and $\boldsymbol{V}$ is the horizontal wind.

$$\frac{\partial w}{\partial z} = -\nabla \bullet \boldsymbol{V} \tag{A.1}$$

The continuity equation is then integrated throughout the depth of the fluid. Looking at (*A*.1), this depth is from $z=h_B$ to $z=\eta$, where h_B is the height of the surface terrain above the reference level $z=0$, and η is the height of the free surface above the reference level $z=0$.

$$\int_{z=h_b}^{z=\eta} \frac{\partial w}{\partial z} dz = \int_{z=h_b}^{z=\eta} -\nabla \bullet \boldsymbol{V} dz \tag{A.2}$$

In a barotropic atmosphere, the winds, and therefore the divergence of the winds, are both invariant with height. Making this assumption, (*A*.2) becomes:

$$w(\eta) - w(h_B) = -(\eta - h_b)\nabla \bullet \boldsymbol{V} \tag{A.3}$$

Using the definition of the total derivative, the left-hand side of (*A*.3) is expanded below.

$$\frac{\partial \eta}{\partial t} + \boldsymbol{V} \bullet \nabla \eta - \left(\frac{\partial h_b}{\partial t} + \boldsymbol{V} \bullet \nabla h_b \right) = -(\eta - h_b)\nabla \bullet \boldsymbol{V} \tag{A.4}$$

The local rate of change of bottom topography $\left(\frac{\partial h_b}{\partial t}\right)$ is treated as zero and vanishes. Applying the above assumption and combining terms on the LHS, we obtain the following equation.

$$\frac{\partial \eta}{\partial t} + \boldsymbol{V} \bullet \nabla \eta - (\eta - h_b) = -(\eta - h_b)\nabla \bullet \boldsymbol{V} \tag{A.5}$$

We now break η into a mean height ($\bar{h}$) above the reference level z=0 seen in (*A*.1) and a perturbation height h', also seen in (*A*.1). Substituting this into the above equation, we obtain the following.

$$\frac{\partial\left(\bar{h}+h'\right)}{\partial t}+\boldsymbol{V}\bullet\nabla\left(\bar{h}+h'-h_b\right)\nabla\bullet\boldsymbol{V} \tag{A.6}$$

Noting that the mean height does not vary with time or space, the above equation simplifies to:

$$\frac{\partial h'}{\partial t}+\boldsymbol{V}\bullet\nabla\left(h'-h_b\right)=-\left(h'-h_b\right)\nabla\boldsymbol{V}-\bar{h}\nabla\bullet\boldsymbol{V} \tag{A.7}$$

Using the following vector expression, where a is an arbitray scalar and $\boldsymbol{V}$ is an arbitrary vector:

$$\nabla\bullet\left(a\boldsymbol{V}\right)=a\nabla\bullet\boldsymbol{V}+\boldsymbol{V}\bullet\nabla a \tag{A.8}$$

Equation (*A*.7) can be rewritten as:

$$\frac{\partial h'}{\partial t}=-\nabla\bullet\left(\left(h'-h_b\right)\boldsymbol{V}\right)-\bar{h}\nabla\bullet\boldsymbol{V} \tag{A.9}$$

Multiplying (*A*.9) by gravity to obtain the equation in terms of geopotential instead of height and substituting "δ" for (∇•$\boldsymbol{V}$), we obtain the geopotential tendency equation used for this study.

$$\frac{\partial\Phi'}{\partial t}=-\nabla\bullet\left(\left(\Phi'-\Phi_b\right)\boldsymbol{V}\right)-\bar{\Phi}\delta \tag{A.10}$$

Appendix B

The Non-linear Balance Equation

The non-linear balance equation is used to initialize a height and wind field while eliminating the initial tendency for gravity wave formation. The equation results from the divergence equation shown below.

$$\frac{\partial \delta}{\partial t} = \hat{\boldsymbol{k}} \bullet \nabla \times (\zeta + f)\boldsymbol{V} - \nabla^2 \left(\Phi + \frac{\boldsymbol{V} \bullet \boldsymbol{V}}{2} \right) \tag{B.1}$$

For more practical use, the divergence equation is expanded below in spherical coordinates.

$$\frac{\partial \delta}{\partial t} = \frac{1}{a(1-\mu^2)} \frac{\partial (v \cos\phi\eta)}{\partial \lambda} - \frac{1}{a} \frac{\partial (u \cos\phi\eta)}{\partial \mu} - \nabla^2 \left(\frac{(u\cos\phi\eta)^2 + (v\cos\phi\eta)^2}{2(1-\mu^2)} \right) - \nabla^2 \Phi \tag{B.2}$$

In (*B*.2), $\mu = sin\phi$ where ϕ represents latitude, λ represents longitude, and η represents the absolute vorticity. To obtain the non-linear balance equation, the local time rate of change of divergence is set to zero, and the Laplacian of the geopotential is solved for.

$$\nabla^2 \Phi = \frac{1}{a(1-\mu^2)} \frac{\partial (v \cos\phi\eta)}{\partial \lambda} - \frac{1}{a} \frac{\partial (u \cos\phi\eta)}{\partial \mu} - \nabla^2 \left(\frac{(u\cos\phi\eta)^2 + (v\cos\phi\eta)^2}{2(1-\mu^2)} \right) \tag{B.3}$$

Equation (*B*.3) appears complicated and would seem difficult to solve without the use of spectral methods. By using the spectral method on a sphere in which the spherical harmonics are eigen functions of the Laplacian operator, the above equation is solved relatively easily given an initial wind field. The result is the initial *perturbation* geopotential field that is in balance with the initial wind field. Note that while the solving for the *perturbation* geopotential is relatively straightforward, the Laplacian operator does prevent the solution of a unique actual geopotential field. This perturbation geopotential field is in balance with the initial wind field, which prevents the development of spurious gravity waves at the start of the simulation. This method was used to initialize all perturbation geopotential fields for the SWM in this study.